"Protection Scheme for Fault Detection, Location and Isolation in DC Ring Microgrid (MATLAB)"

[1]Sunil D Kanoje , [2]Dr. Nilesh P. Bodne , [3]Prof. Kiran M, Kimmatkar, [4]Prof. Manjit Sakhare
[1] Student of VIT, Nagpur, [2,3,4] Professor of VIT, Nagpur, Professor of VIT, Nagpur,
Department of Electrical Engineering,
Vidarbha Institute Of Technology, Nagpur, Maharashtra, India.
[1]sunilkanoje92@gmail.com,

Abstract
This article introduces a centralized protection system design for DC micro grade. The Novelty of this protection algorithm lies not only in the combination of different false location but also in its fault characterization approach full stop the protection system was developed based on monitoring voltage and current various point will in the DCMG. Upon detecting fault using specific criteria, protective measures are initiated, and appropriate switching signal are same to the corresponding solid state circuit breaker (SSCB) to isolate the faulty section. The study involves simulating and 96-volt DCMG with a ring configuration using the MATLAB/Simulink environment. The simulation result demonstrates the effectiveness of the propose method in identifying fault within the DCMG.
Index terms: DC Microgrid (DCMG), centralized protection, fault analysis cumulative and some average technique, SSCB (Keywords)

INTRODUCTION

DC microgrid offer significant advantage over AC microgrids, including cost -effectiveness, enhanced reliability, higher efficiency, and greater scalability. This makes them particularly advantageous for remote locations such as rural, tribal, and hilly areas. In this regions, establishing a grid connected sub-system can be prohibitively expansive due to the high costs involved in setting up a sub-station with transformer and other heavy equipment's. However, opting for a smaller Solar DC microgrid (DCMG) proves to be a more financially viable and sensible option.

1. Study of state-of-the-art protection schemes

DC Microgrids (DCMGs) are widely applicable in various fields such as telecommunications, navy shipboard bases, data centers, automotive, and rural areas due to their high efficiency, minimal power loss, and increased power handling capacity [1]. However, protecting DCMGs connected with distributed renewable energy sources (DERs), energy storage systems (ESSs), and critical/non-critical loads from different faults poses a significant challenge for researchers. In multi-agent dynamic networks like DCMGs, the existing protective mechanisms often struggle with effective fault detection and isolation. Incorrect determination of the fault section can lead to unreliable fault clearing [2].
The potential faults in DCMGs include line-to-ground faults and line-to-line faults. Line-to-ground faults are more common and occur due to aging, physical contact deterioration, or live part connections to the ground. Some existing protection schemes, such as a differential current protection scheme described in [3], require high communication channels for data transfer, making them susceptible to failure when the communication network faces issues.
In [4], the detection of DC faults using a hybrid-passive overcurrent relay with a discrete wavelet transform is proposed, but it lacks precise selectivity among protection devices. Another approach in [5] involves detecting and locating faults based on the direction of the current flow. An active impedance-based fault location method for DC systems is expressed in [6], but it becomes complex to detect the location of resistive faults due to the rapid rate of current change.
Some research, like that in [7], explores traveling wave fault detection for DCMGs, but it requires additional tools to speed up the receiving data.

2. Contribution of this Article

In summary, the article reviews state-of-the-art protection schemes for DCMGs, analyzing their fundamental operating principles, operating times, and usages.
This article focuses on a five-bus 96V DC microgrid (DCMG) and implements a centralized protection system to address various fault and overload conditions. The protection system is designed to cover bus bar faults, short circuits, open circuit line faults, and overload situations. A specially designed impedance slope-based protection scheme is employed in this study.
The protection algorithms are developed using cumulative sum average techniques. To isolate the faulty section, Solid State Circuit Breakers (SSCBs) are utilized. The researchers test the system under diverse contingency conditions to ensure its reliability and effectiveness.
The results of the proposed DCMG fault detection, location, and isolation system are found to be satisfactory, indicating its successful performance in safeguarding the microgrid from faults and overload scenarios.

DEVELOPMENT OF DCMG PROTECTION SYSTEM

1. DCMG Architecture

The DCMG studied in this research is a 96V DC ring microgrid comprising various components, as illustrated in Fig.1. The microgrid includes distributed generation in the form of two solar PV arrays, each with a capacity of 4 kW. These PV arrays supply power to both critical and non-critical DC loads, totaling 5 kW.
An energy storage system, represented by a battery, is also integrated into the microgrid. The battery serves the dual purpose of storing excess energy from the PV arrays and providing backup power when needed.
The microgrid is structured as a five-bus system, with five line segments connecting the buses. Each bus is equipped with a voltage sensor to measure the voltage at that specific point. Additionally, each line segment has two current sensors installed in such a way that they

detect positive current values whenever there is current flow from the bus bar.

Protection Scheme	Principal	Operating time	Application	Configuration	Ref.
Measurment Baesd					
Over Current	$I > I_{th}$	<2 ms for low impedance faults and <5 ms for high impedance faults	Fault detection	LVDC test grid based on IEEE 14 bus system and interconnected topology	[8]
$\frac{di}{dt}$	$I_{diff} > \frac{di}{dt}$	<0.1ms for metallic faults and <0.2 ms for high impedance faults	Fault detection	Network or ring topology	[9]
Voltage Estimation	$\Delta I > \Delta I_{th}$	<300 ms from fault detection to isolation	Fault detection, location and isolation	Network or ring topology	[10]
Handshaking	$\Delta I > \Delta I_{th}$	< 300 ms from fault detection to isolation	Fault detection, location and isolation	Network or ring topology	[11]
Communication Based					
Differential	$I_{diff} > \Delta I_{th}$	<0.2 ms	Fault detection, and isolation	Network or ring topology and single bus	[3],[12]
Artificial Inductive	$\frac{di}{dt}$	<30 ms from fault detection to isolation	Fault detection, location and isolation	Fault detection, location and isolation	[13]
Active distance estimation	$\frac{di}{dt}$ and $\Delta I > \Delta I$ th	<60 ms from fault detection to isolation	Fault detection, location and isolation	Network or ring topology	[14]

Table 1 DIFFERENT PROTECTION SCHEME

System Voltage	96V
Solar Panel	Vmp=29V, Imp=7.35A at STC
PV Panel- 1	4000W
Load- 1 (Critical)	1500W
Load- 2 (Non-Critical)	3500W
Battery (ESS)	96V, 20Ah
DC link Capacitor	5mF
Line resistance	0.143 Ω/km
Line inductance	0.5 mH/km

Table 2 Parameters for DCMG

In summary, the DCMG consists of a 96V DC ring microgrid with solar PV arrays, an energy storage system, and various DC loads. It operates as a five-bus system with voltage sensors at each bus and current sensors at each line segment, ensuring efficient monitoring and control of the power distribution within the microgrid.

The PV solar sources in this study are modelled assuming a constant array temperature of 25°C and a solar irradiance level of 1000W/m^2. These assumptions are used to obtain the current-voltage (I-V) characteristics of the PV array model. To optimize the power output from the PV sources, the Incremental Conductance algorithm is employed for Maximum Power Point Tracking (MPPT). This algorithm adjusts the duty cycle of the transistor's gate valve at a frequency of 5 kHz to achieve the desired voltage and deliver maximum power from the PV array.

To step up the power from the PV array's 24V output to the required 96V for the DCMG, DC-DC boost converters are used. These boost converters facilitate the voltage transformation process and enable efficient power transfer within the microgrid.

The specific parameters of the DCMG, beyond those mentioned, are not provided in the current context. However, the DCMG's overall performance is likely to be

influenced by factors such as its load characteristics, battery capacity, power demand profile, and the control mechanisms governing its operation.

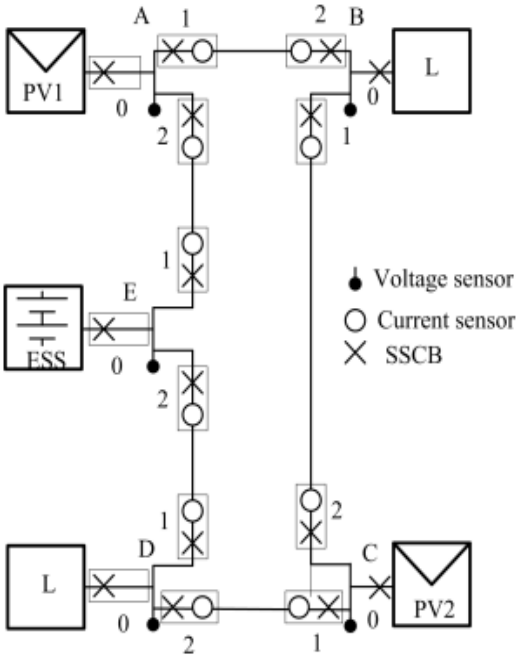

Fig 1 DCMG

2. Problem Statements

The problem addressed in this study involves developing a cost-effective, reliable, and rapid protection system for a 96V DC microgrid (DCMG) to safeguard against various fault conditions. The protection scheme aims to detect and isolate short circuit line and bus faults, open circuit line faults, and overload situations throughout the entire DCMG. To achieve this, the proposed protection system incorporates five voltage sensors and ten current sensors placed strategically within the microgrid.

The centralized protection system continuously collects voltage and current data from these sensors. Based on the protection algorithm, which relies on the cumulative sum average technique, the system determines the type of fault present and issues a trip signal to the corresponding Solid State Circuit Breaker (SSCB) to isolate the faulty section in the DCMG.

During steady-state conditions, when time t is negligible, the inductance in the system is minimal, and the voltage across bus B is given by the

$$v_B(t) = v_C(t) + i_{BC}(t)R_{BC} \qquad (1)$$

sum of the voltage at bus C and the product of current i_{BC} and resistance R_{BC} for the section BC, as shown in Fig.2(a). However, during transient conditions at time t_1, the effect of inductance L_{BC} causes an increase in the voltage drop across the line BC altered voltage at bus B due to a forward fault at time t_2 can be expressed as follows:

$$v_B(t_1) = v_C(t_1) + i_{BC}(t_1)R_{BC} + L_{BC}\frac{di_{BC}}{dt} \qquad (2)$$

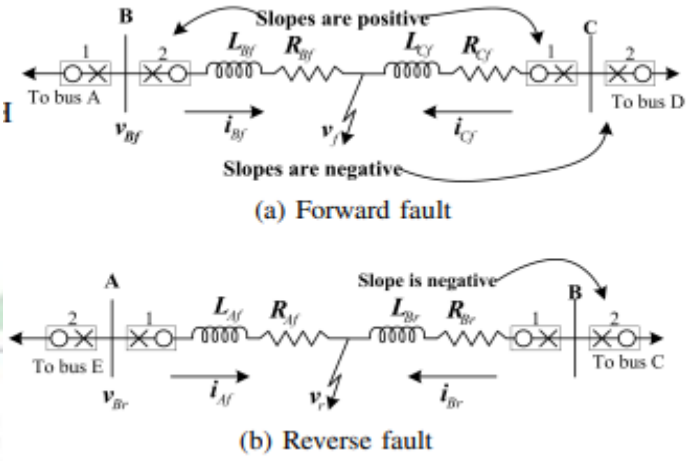

Fig 1

For a reverse fault at time t3, the voltage at bus B, denoted as $v_B(t3)$, will be affected by the fault current i_F and the impedance of the fault path, represented by ZF. The altered voltage at bus B for a reverse fault is given by:

$$v_{Bf}(t_2) = v_f(t_2) + i_{Bf}(t_2)R_{Bf} + L_{Bf}\frac{di_{Bf}}{dt} \qquad (3)$$

Where, v_Bf and v_f are the voltages at bus B and at fault point f respectively. Also, i_{Bf} , R_{Bf} and L_{Bf} are the current, resistance and inductance of the section BC up to fault point f respectively. However, for reverse fault seen by the same relay located at bus B shown in Fig. 2(b), the voltage at bus B at time instant t3 is given as,

This expression represents the altered voltage at bus B during a reverse fault at time t3. It considers the impact of the fault current and the impedance of the fault path on the voltage at bus B during the transient condition caused by the reverse fault.

$$v_{Br}(t_3) = v_r(t_3) + i_{Br}(t_3)R_{Br} + L_{Br}\frac{di_{Br}}{dt} \qquad (4)$$

change in voltage for three different conditions in the DCMG can be determined using the following expressions:

Transient condition - Change in voltage (Δv_T):

$\Delta v_T = v_B(t_1) - v_B(t)$

$= (v_C(t_1) + i_{BC}(t_1) * R_{BC} + L_{BC} * (di_{BC}/dt)|t1) - (v_C(t) + i_{BC}(t) * R_{BC})$

Forward fault - Change in voltage (Δv_F):

$\Delta v_F = v_{Bf} - v_B(t)$

$= (v_{Cf} + i_{Bf} * R_{BC} + L_{Bf} * (di_{BC}/dt)|t_2 + i_F * Z_F) - (v_C(t) + i_{BC}(t) * R_{BC})$

Reverse fault - Change in voltage (ΔvR):

$\Delta v_R = v_{Br} - v_B(t)$

$= (v_{Cr} + i_{Br} * R_{BC} + L_{Br} * (di_{BC}/dt)|t_3 - i_F * Z_F) - (v_C(t) + i_{BC}(t) * R_{BC})$

Where: $v_B(t_1)$ is the altered voltage at bus B during the transient condition at time t_1. $v_B(t)$ is the voltage at bus B during steady-state conditions (no fault). $v_C(t1)$ is the voltage at bus C during the transient condition at time t_1. $i_{BC}(t_1)$ is the current flowing through the section BC during the transient condition at time t_1. RBC is the resistance of

the section BC. LBC is the inductance of the section BC. $(di_{BC}/dt)|t_1$ is the rate of change of current through the section BC at time t_1. v_{Bf} is the altered voltage at bus B during the forward fault. v_{Cf} is the voltage at bus C during the forward fault. i_{Bf} is the fault current during the forward fault. Z_F is the impedance of the fault path during the forward fault. v_{Br} is the altered voltage at bus B during the reverse fault. v_{Cr} is the voltage at bus C during the reverse fault. i_{Br} is the fault current during the reverse fault. L_{Bf} is the inductance of the section AB up to fault point r during the forward fault. L_{Br} is the inductance of the section AB up to fault point r during the reverse fault.

These expressions allow the determination of voltage changes for each condition (transient, forward fault, and reverse fault) and are essential in understanding the behavior of the DCMG under different fault scenarios.

$$\Delta v_F = v_{Bf}(t_2) - v_B(t)$$

$$\Delta v_F = \left(v_f(t_2) + i_{BCf}(t_2)R_{BCf} + L_{BCf}\frac{di_{BCf}}{dt}\right) - (V_C(t) + i_{BC}(t)R_{BC}) \quad (5)$$

In the case of a reverse fault, the change in voltage (Δv_R) is indeed given as the difference between equation (4) and equation (1). It is expressed as follows:

$$\Delta v_R = v_{Br}(t_2) - v_B(t)$$

$$\Delta v_R = \left(v_{fr}(t_3) + i_{ABfr}(t_3)R_{ABf} + L_{ABf}\frac{di_{ABfr}}{dt}\right) - (V_C(t) + i_{BC}(t)R_{BC}) \quad (6)$$

Where: v_{Br} is the altered voltage at bus B during the reverse fault. v_{Cr} is the voltage at bus C during the reverse fault. i_{Br} is the current flowing through the section AB up to fault point r during the reverse fault. L_{Br} is the inductance of the section AB up to fault point r during the reverse fault. $(di_{BC}/dt)|t_3$ is the rate of change of current through the section BC at time t_3. $v_C(t)$ is the voltage at bus C during steady-state conditions (no fault). $i_{BC}(t)$ is the current flowing through the section BC during steady-state conditions (no fault). RBC is the resistance of the section B_C. i_F is the fault current during the reverse fault. Z_F is the impedance of the fault path during the reverse fault.

This expression provides the voltage change (Δv_R) at bus B during a reverse fault compared to the steady-state condition (no fault). It considers the impact of the fault current and the impedance of the fault path on the voltage at bus B during the transient condition caused by the reverse fault.

Change in magnitude of current for transient condition (Δi_T): $\Delta i_T = i_{BC}(t_1) - i_{BC}(t)$ (Equation 7)

Change in magnitude of current for forward fault (Δi_F): $\Delta i_F = i_{Bf}(t_2) - i_{BC}(t)$ (Equation 8)

Change in magnitude of current for reverse fault (Δi_R): $\Delta i_R = i_{Br}(t_3) - i_{BC}(t)$ (Equation 9)

Change in voltage at bus B for open circuit fault (Δv_O): $\Delta v_O = v_{BO}(t4) - v_B(t)$ (Equation 10)

From Equations 5 to 9, the ratio of change in voltage and current gives the slope for three distinct conditions: transient, forward fault, and reverse fault. These slopes are equivalent to the impedances and are expressed as:

$\Delta Z_T = \Delta v_T / \Delta_{iT}$ (Equation 11)

$\Delta Z_F = \Delta v_F / \Delta_{iF}$ (Equation 12)

$\Delta Z_R = \Delta v_R / \Delta i_R$ (Equation 13)

In the case of an open circuit fault, the line current becomes zero, and the slope (ΔZO) tends to infinity or very high:

$\Delta Z_O = \Delta v_B / \Delta i_R \rightarrow 0$ (Equation 14)

The proposed protection algorithm determines the slope using Equations 11 to 14. Based on these slopes, specific time windows are defined, as shown in Fig.3. These time windows aid in detecting and identifying various fault conditions in the DCMG, allowing the protection system to respond appropriately and isolate the faulty section.

3. Proposed Protection Algorithm

Fig.4 shows the proposed protection algorithm for the DCMG with different faults. The centralized protection system analyzes various fault conditions and observes and notes the slopes at both ends of every line segment during a fault condition. The algorithm categorizes forward and reverse faults based on the respective slopes observed at both ends of the faulted line.

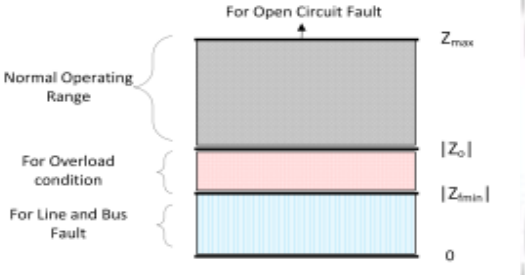

Fig. 3. Variation in impedance

Specifically, the slopes are positive for the line fault section and negative for the bus fault section for the corresponding line and bus sensors. By examining the nature (positive or negative) of the slopes, the algorithm identifies the direction of the fault location. Once the direction of the fault is determined, the protection system issues a trip command to the associated Solid State Circuit Breaker (SSCB) to isolate the faulty section effectively.

In summary, the proposed algorithm utilizes slope analysis and fault direction identification to determine the type and location of faults in the DCMG. This enables the protection system to take appropriate actions in response to different fault scenarios and ensure reliable and fast protection for the entire DC microgrid.

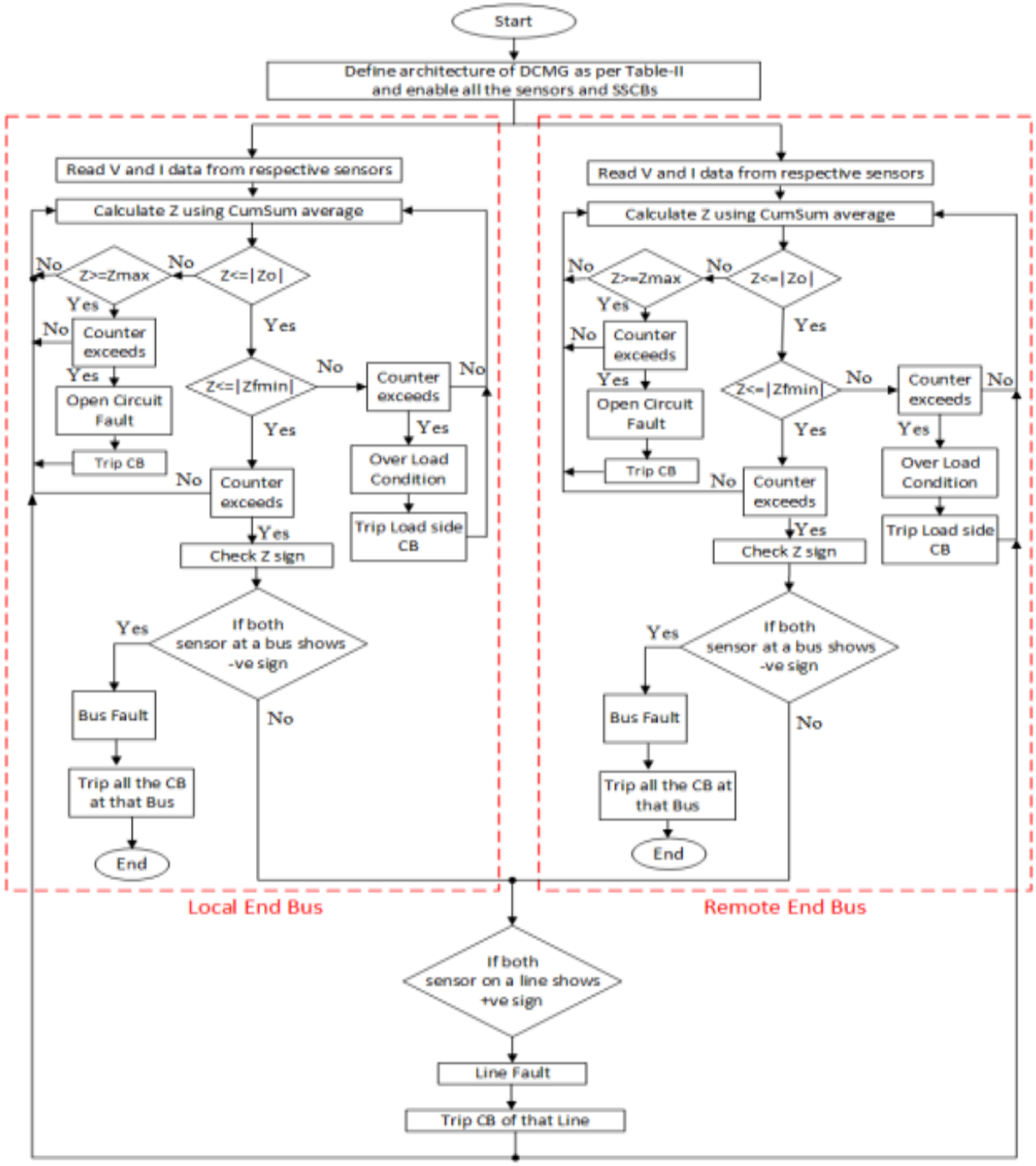

Fig. 4. Flowchart of proposed protection scheme

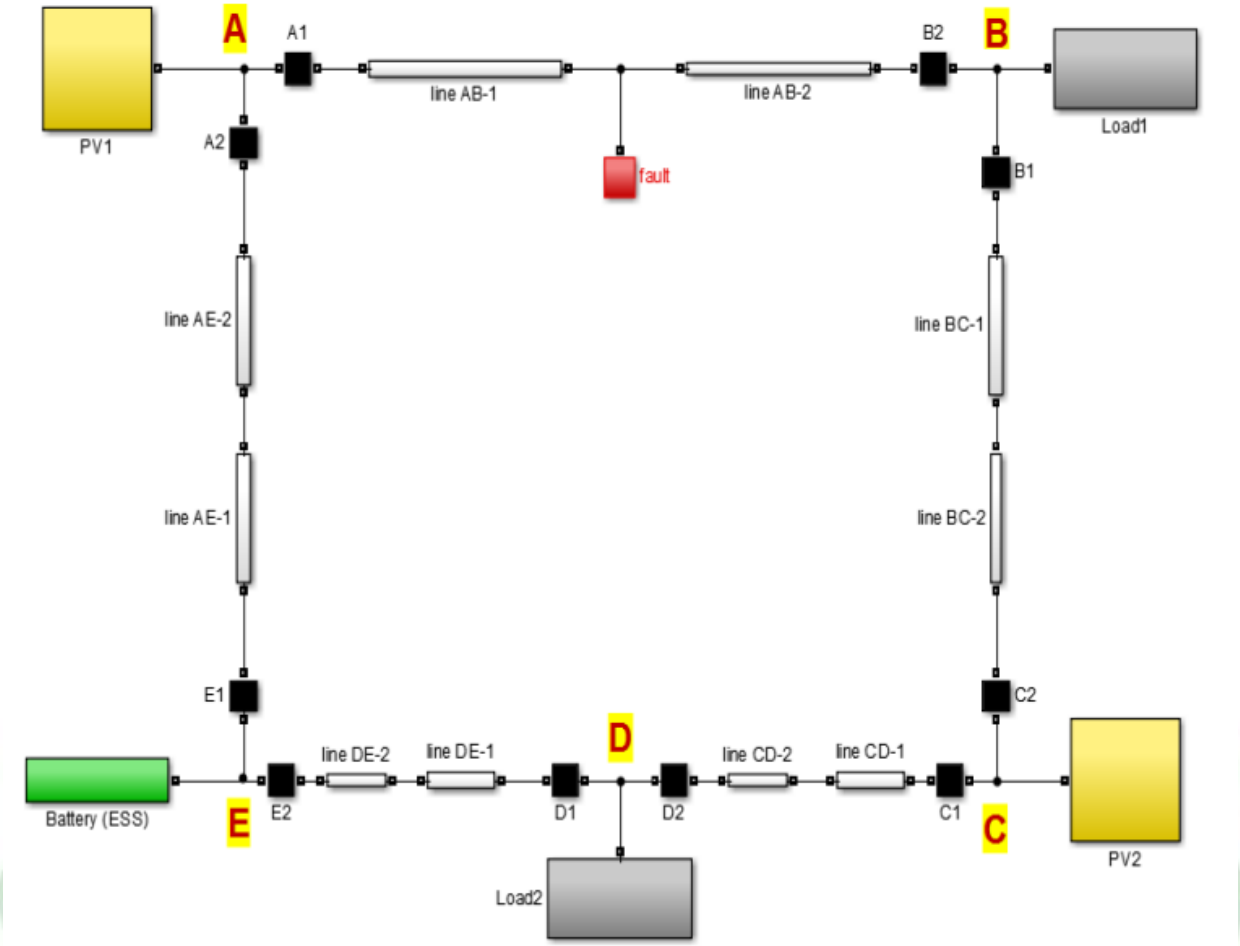

Fig 5: DCMG system simulated in MATLAB/Simulink

Result

The DCMG System simulated in MATLAB/Simulink is shown in Fig. 5

Case-I: Performance of the proposed system under normal condition

The system is tested for different operational conditions without any faults. These conditions include:

(a) ESS is charging: Initially, the Energy Storage System (ESS) is in the charging mode. It draws current from the microgrid to store energy. The charging process continues until the ESS is completely charged.

(b) ESS is floating: At 0.1 seconds, the ESS reaches its fully charged state. During this time, the ESS is neither drawing current from the microgrid nor supplying any current, resulting in a floating state.

(c) ESS is discharging: At 0.2 seconds, more loads are connected to the system, causing the ESS to enter the discharging mode. The ESS starts supplying current from its stored energy to meet the increased load demand.

The respective simulation waveforms depict how the system behaves under these different conditions. These waveforms show the variations in voltage, current, and other relevant parameters as the ESS undergoes charging, floating, and discharging states. The waveforms provide valuable insights into the dynamic behaviour and performance of the system under varying load and ESS conditions.

Case-II: Performance of the proposed system under over load condition

The proposed protection algorithm continuously monitors the system's data. When an overload condition occurs at 0.2 seconds, the slope value starts to decrease below a predefined threshold. The algorithm observes the slope value and checks if it remains below the predefined threshold for a specific interval of time.

If the slope value remains below the predefined threshold for this interval, it indicates a potential overload situation. In response, the protection system initiates trip commands for the Solid-State Circuit Breaker (SSCB) located at the Load side (B0). By doing so, the Load section is isolated, protecting the rest of the system from potential overload damage.

The simulation waveforms show the effect of this protection action on A1, likely demonstrating the stability and safety of the system after isolating the Load section. The waveforms would indicate changes in voltage, current, and other relevant parameters during this process.

In summary, the algorithm's continuous monitoring of the slope value allows the protection system to detect and respond promptly to overload conditions, effectively isolating the affected Load section and preventing any adverse effects on the rest of the system. The simulation waveforms provide visual evidence of the algorithm's effectiveness in ensuring the stability and protection of the DCMG.

Case-III: Performance of the proposed system for line fault condition

In response to the line-to-ground fault created at 0.2 seconds between Bus A and B, the protection algorithm reads the data and determines the slopes at both ends, A1 and B2, respectively. According to Table-III, it is observed that after the fault between Bus A and Bus B, the slopes at A1 and B2 are positive and less than the defined value, which signifies the occurrence of a fault.
Based on this determination, the protection system initiates trip commands for Solid State Circuit Breakers (SSCB) A1 and B2. This action isolates the faulty line section effectively, preventing further damage and ensuring the safety of the system.
The simulation results for SSCB A1 are depicted in Fig.8, likely showing the behaviour of voltage, current, and other parameters at A1 during the fault and after the protection system's response.
In summary, the protection algorithm's ability to detect the line-to-ground fault based on the slopes at both ends of the faulty line section enables it to promptly initiate trip commands for the relevant SSCBs, leading to the successful isolation of the faulty section. The simulation results in Fig.8 provide visual evidence of the protection system's effectiveness in mitigating the impact of the fault at A1.

Case-IV: Performance of the proposed system under Bus fault condition

In the scenario where the ground fault is established at Bus B, the direction of current gets reversed for section CD. The protection algorithm reads the data and determines the slopes at locations B1 and B2. As per Table-III, it is observed that after the ground fault at Bus B, the slopes at B1 and B2 are negative and less than the predefined value, indicating the occurrence of a fault.
Based on this determination, the protection system initiates trip commands for Solid State Circuit Breakers (SSCB) B1 and B2. This action isolates the faulty bus section effectively, preventing further issues and ensuring the safety of the system.
The simulation results for SSCB B2 are depicted in Fig.9, likely showing the behaviour of voltage, current, and other parameters at B2 during the fault and after the protection system's response.
In summary, the protection algorithm's capability to detect the ground fault and reversed current direction in section CD allows it to promptly initiate trip commands for the relevant SSCBs, leading to the successful isolation of the faulty bus section. The simulation results in Fig.9 provide visual evidence of the protection system's effectiveness in mitigating the impact of the ground fault at B2.

Case-V: Performance of the proposed system under open circuit fault condition

In response to the open circuit fault created at 0.2 seconds between Bus A and B, the protection algorithm reads the data and determines the slopes at both ends, A1 and B2, respectively. As per the observation, the slopes at A1 and B2 are more than the predefined value, indicating the occurrence of an open circuit fault.
Based on this determination, the protection system initiates trip commands for Solid State Circuit Breakers (SSCB) located at A1 and B2. This action isolates the faulty section effectively, preventing any further issues and ensuring the safety of the system.
The simulation results for SSCB B2 are depicted in Fig.10, likely showing the behaviour of voltage, current, and other parameters at B2 during the fault and after the protection system's response.
In summary, the protection algorithm's capability to detect the open circuit fault based on the slopes at both ends of the faulty section allows it to promptly initiate trip commands for the relevant SSCBs, leading to the successful isolation of the faulty section. The simulation results in Fig.10 provide visual evidence of the protection system's effectiveness in mitigating the impact of the open circuit fault at B2.
The article proposes a protection scheme algorithm for a five-bus DC ring microgrid (DCMG) with a voltage level of 96V. The DCMG includes two PV solar distributed generation sources, an Energy Storage System (ESS), and critical/non-critical loads. The protection algorithm is based on the slope impedance technique.

CONCLUSION

The proposed protection algorithm has been extensively tested for various fault types occurring at different locations within the DCMG. These fault types include line-to-ground faults, open circuit faults, and forward and reverse faults. The algorithm effectively analyses the slopes and impedance at different points within the microgrid to detect and classify fault conditions accurately.
The key features of the proposed protection system are:
Simplicity: The algorithm's design and implementation are straightforward, making it easy to understand and maintain.
Speed: The protection system responds rapidly to fault conditions, ensuring quick isolation of the faulty sections and preventing further damage.
Suitability: The protection system is well-suited for safeguarding the DCMG from various types of faults without causing disruptions to the normal operation of the grid.
Reliability: By promptly detecting and isolating faults, the proposed protection algorithm ensures the reliable operation of the DCMG even during abnormal conditions.
Overall, the article presents a practical and efficient protection scheme for a DC microgrid, offering increased system stability, improved fault management, and enhanced grid resilience. The proposed protection system's ability to respond swiftly and accurately to different fault scenarios contributes to the overall reliability and safety of the DCMG.

REFERENCES

[1] Dinesh Kumar, Arindam Ghosh, "DC Microgrid Technology: System Architectures, Communication Networks, Applications and Standardizations Aspects," IEEE Proc.,2017.

[2] J. Park, J. Candelaria, L. Ma, and K. Dunn, "DC Ring-Bus Microgrid Fault Protection and Identification of Fault Location," IEEE Trans. Power Deliv., vol. 28, no. 4, pp. 2574–2584, Oct. 2013.

[3] Steven D. A. Fletcher, Patrick J. Norman, Stuart J. Galloway, and Graeme M. Burt, "High-Speed Differential Protection for Smart DC Distribution Systems," IEEE Transactions on Smart Grid, Vol. 5, Issue.5, Sept 2014.

[4] Khaled A. Saleh, Ali Hooshyar and Ehab F. El-Saadan, "Hybrid PassiveOver current Relay for Detection of Faults in Low-Voltage DC Grids," IEEE Transaction on Smart Grid, Vol.8, Issue.3, May 2017.

[5] Abdullah A. S. Emhemed, Steven Fletcher, and Graeme M. Burt, "Validation of fast and selective protection scheme for an LVDC distribution network," IEEE Transactions on Power Delivery, Vol.32, Issue.3, June 2017.

[6] Edward Christopher, Mark Sumner, David W.P. Thomas, "Fault location in a zonal DC marine power system using Active Impedance Estimation," IEEE Transactions on Industry Applications, Vol.49, Issue.2, Mar.2013.

[7] Sadegh Azizi, Majid Sanaye Pasand, Moein Abedini and Abbas Hasani, "A Traveling-Wave Based Methodology for Wide-Area Fault Location in Multiterminal DC Systems," IEEE Transactions on Power Delivery., vol. 29, Issue.6, Dec. 2014.

[8] K. A. Saleh, A. Hooshyar, and E. F. El-Saadany, "Hybrid PassiveOvercurrent Relay for Detection of Faults in Low-Voltage DC Grids," IEEE Trans. Smart Grid, vol. 8, no. 3, pp. 1129–1138, May 2017.

[9] A. Meghwani, S. C. Srivastava, S. Member, S. Chakrabarti, and S. Member, "A Non-unit Protection Scheme for DC Microgrid Based on Local Measurements," vol. 32, no. 1, pp. 172–181, 2017.

[10] A. Meghwani, S. Chakrabarti, and S. C. Srivastava, "A Fast Scheme for Fault Detection in DC Microgrid Based on Voltage Prediction." 2016 National Power Systems Conference (NPSC) , IIT Bhubaneswar, 19-21 December 2016.

[11] L. Tang and B. Ooi, "Locating and Isolating DC Faults in MultiTerminal DC Systems," vol. 22, no. 3, pp. 1877–1884, 2007.

[12] J. Park, J. Candelaria, L. Ma, and K. Dunn, "DC Ring-Bus Microgrid Fault Protection and Identification of Fault Location," IEEE Trans. Power Deliv., vol. 28, no. 4, pp. 2574–2584, Oct. 2013.

[13] M. Farhadi and O. A. Mohammed, "Event-Based Protection Scheme for a Multiterminal Hybrid DC Power System," IEEE Trans. Smart Grid, vol. 6, no. 4, pp. 1658–1669, Jul. 2015.

[14] K. Jia, E. Christopher, D. Thomas, M. Sumner, and T. Bi, "Advanced DC zonal marine power system protection," no. June 2013, pp. 301–309, 2014.